PROTEINS: Structure, Function, and Genetics 33:145–158 (1998)

RESEARCH ARTICLES

Improving the Accuracy of Protein pK_a Calculations: Conformational Averaging Versus the Average Structure

Herman W.T. van Vlijmen,[1] Michael Schaefer,[1,2] and Martin Karplus[1,2]*
[1]*Department of Chemistry and Chemical Biology, Harvard University, Cambridge, Massachusetts*
[2]*Laboratoire de Chimie Biophysique, Institut le Bel, Université Louis Pasteur, Strasbourg, France*

ABSTRACT **Several methods for including the conformational flexibility of proteins in the calculation of titration curves are compared. The methods use the linearized Poisson-Boltzmann equation to calculate the electrostatic free energies of solvation and are applied to bovine pancreatic trypsin inhibitor (BPTI) and hen egg-white lysozyme (HEWL). An ensemble of conformations is generated by a molecular dynamics simulation of the proteins with explicit solvent. The average titration curve of the ensemble is calculated in three different ways: an average structure is used for the pK_a calculation; the electrostatic interaction free energies are averaged and used for the pK_a calculation; and the titration curve for each structure is calculated and the curves are averaged. The three averaging methods give very similar results and improve the pK_a values to approximately the same degree. This suggests, in contrast to implications from other work, that the observed improvement of pK_a values in the present studies is due not to averaging over an ensemble of structures, but rather to the generation of a single properly averaged structure for the pK_a calculation. Proteins 33:145–158, 1998.** © 1998 Wiley-Liss, Inc.

Key words: protein titration; molecular dynamics; average conformation; continuum electrostatistics; protein dielectric constant

INTRODUCTION

The importance of the effect of pH on the structure and function of macromolecules of biological interest is well known.[1–5] The pH-dependent effects in proteins are predominantly electrostatic and originate from changes in the protonation states of acidic and basic residue sidechains. The effects include changes in catalytic activity,[6] in ligand binding,[7] and in protein stability.[8–11] Many titratable residues display different titration behavior in the native protein compared to that of the isolated residue in solution. This is caused by differences in the electrostatic environment of the residue. There are two types of contributions to the difference. The first arises from the interaction with polar groups and other titratable residues in the protein, and the second from an altered interaction with the solvent (Born correction); i.e., the residue is part of a low dielectric constant environment.

Since the work of Linderstrøm-Lang,[12] methods have been devised to introduce these two effects and to calculate the titration behavior of proteins. Linderstrøm-Lang treated a protein as a low dielectric sphere with a uniformly charged surface surrounded by a high dielectric continuum. As a consequence of the uniform charge assumption, this model could treat only the average titration behavior and did not provide information about the titration of individual residues. Tanford and Kirkwood[13] also used a spherical model, but introduced discrete unit charges on the surface; with this model, which was developed further by Gurd and coworkers,[14] they were able to calculate the titration behavior as a function of the locations of the titratable sites. Advances in computation power have made it possible to depart from the spherical protein model, and treat a protein structure at the atomic level by solving the linearized Poisson-Boltzmann (LPB) equation numerically,[15–18] or by use of microscopic polarization methods.[19] The first detailed calculation of the titration behavior of individual residues using the LPB equation and

Herman W.T. van Vlijmen's present address is Biogen, Inc., 14 Cambridge Center, Cambridge, MA 02142.
*Correspondence to: Martin Karplus, Laboratoire de Chimie Biophysique, Institut le Bel, Université Louis Pasteur, 4, Rue Blaise Pascal, 67000 Strasbourg, France. E-mail: marci@brel.u-strasbg.fr
Received 7 November 1997; Accepted 25 June 1998

taking into account all possible protonation states of the system was made by Bashford and Karplus.[20,21] Similar calculations have been used to predict pH-dependent folding stabilities,[11,22,23] and to elucidate the mechanisms of bacteriorhodopsin[24] and the bacterial photosynthetic reaction center.[25]

The methods in current use determine the pH-dependent free energy for all important protonation states of the protein,[21] and do a Boltzmann weighted sum over all states to obtain the average degrees of protonation for every residue within a certain pH interval. An alternative approach, which is based on the assumption of Gaussian fluctuations in the total solute-solvent electrostatic interaction energy that are estimated from a molecular dynamics simulation of a solvated protein, has not yet been shown to yield results of comparable accuracy.[26]

Although the overall theoretical framework for calculating pK_a's in proteins is well-defined, in principle, there are several factors in the actual pK_a calculations that introduce significant uncertainties. They include the values of the (partial) atomic charges, the van der Waals radii,[27] which determine the molecular surface, the dielectric "constant" distribution of the protein interior,[28] whether explicit waters should be included in describing the dielectric boundary,[29] and the adequacy of a single crystal structure to represent the ensemble of conformations that exists in solution.[20] The role of a number of these factors has been examined.

Following Lim et al.,[27] Sitkoff et al.[30] adjusted atomic charges and radii by fitting to experimental solvation energies of small organic molecules. Bruccoleri[31] suggested a method in which the atomic charges are not represented as points but as spheres of uniform charge. This method reduced the dependence of the finite-difference calculation on the positioning of the grid. Oberoi and Allewell[32] found better agreement of the calculated pK_a's with experimental results when the net charge of ionized sidechains was placed on the most solvent-exposed atom. Another approach used atomic radii based on the radial distribution function of water around the atoms.[33] Yang et al.[34] found that inclusion of bound waters in the vicinity of a salt bridge in T4 lysozyme improved the prediction of the titration behavior of the residues involved. Recently, Gibas and Subramaniam[29] did a systematic study to determine the number of bound waters that should be included to best predict the pK_a's in HEWL. They concluded that approximately one water molecule within hydrogen-bonding distance should be included for each charged sidechain. Antosiewicz et al.[23] suggested the use of an internal protein dielectric constant of 20, much higher than the generally accepted value of 2–4.[4] They reasoned that the high dielectric constant compensates for the omission of local conformational changes and specific ion binding. Schaefer et al.[11] varied the protein dielectric constant in the range from 1 to 30, and found that a value of 20 leads to the best results for HEWL. States and Karplus[35] proposed the use of different values of the dielectric constant for protein interior and surface residues in the framework of the Tanford and Kirkwood model. The idea was taken up recently by Demchuk and Wade[36] in a modified form; they did separate LPB calculations for the surface groups and buried sites, using protein dielectric constants of 80 and 15, respectively; buried sites were identified based on the magnitude of the charge-solvent energy.

Conformational variability may have a substantial effect on electrostatic interactions.[37,38] Bashford and Karplus[20] showed that for particular residues in HEWL, different residue conformations produced large shifts in the predicted pK_a values. Langsetmo et al.[39] generated an ensemble of sidechain conformations of Lys 57 in thioredoxin, and could thus explain the unexpectedly low pK_a of Asp 26. Bashford and Gerwert[24] used an ensemble of bacteriorhodopsin conformations generated by a molecular dynamics simulation, and calculated average pK_a values by averaging the pK_a's of the ensemble members. The averaging procedure seemed to improve the results somewhat, although it should be noted that the experimental pK_a's are not well-defined. Yang and Honig,[22] Oberoi and Allewell,[32] Bashford et al.,[40] and Antosiewicz et al.[23] calculated pK_a's of proteins based on several different crystal structures and/or protein forms, and found significant differences in predicted pK_a's. Recently, You and Bashford[41] reported a method in which they sampled several sidechain conformations for titratable residues and averaged the electrostatic solvation and interaction energies over the set of conformations for each residue separately. They found better agreement with experimental results and a lower sensitivity to the particular crystal structure on which the calculations were based. Beroza and Case[42] improved the accuracy of pK_a predictions by using a method in which sidechains could exist in two alternative conformations; one taken from the crystal structure and the other a fully extended conformation. Alexov and Gunner[43] included protein flexibility by coupling changes in protonation states of residues to reorientation of neighboring hydroxyl dipoles. While this work was in progress, Zhou and Vijayakumar[44] reported a pK_a calculation method similar to the method of Bashford and Gerwert,[24] in which a set of 14 conformations of cytochrome C was generated with molecular dynamics. Average pK_a's were determined by averaging the titration curves of the titratable residues over all protein conformations. Comparison to experimental pK_a's was limited to three residues, and possible improvements over the single conformation method were not determined.

In this report we compare methods which explicitly account for conformational variability. The approach is similar to the one used by Bashford and

Gerwert,[24] but the conclusion is different. We create an ensemble of protein conformations by extracting structures from molecular dynamics trajectories. We then average the results of all members using three different averaging methods. They include averaging of the structures, the electrostatic energies, and the titration curves. The methods are applied to BPTI and HEWL.

METHODS

Calculation of pK_a Values

The methods used for calculating the titration curves of proteins have been reviewed elsewhere.[11,21,34] They are based on the calculation of the pH-dependent electrostatic energy of each individual protonation state, followed by a Boltzmann-weighted ensemble averaging over all states to obtain the average degree of protonation of the titratable sites. Given a protein with N titratable sites, the protonation state can be described by a vector **s** with components $s_i (i = 1, \ldots, N)$, where s_i equals 0 if site i is unprotonated, and 1 if it is protonated; it is assumed here that each residue has only a protonated and unprotonated state. It has been shown that the pH-dependent free energy difference between the protein in protonation state **s** and the fully unprotonated state is given by[11]

$$\Delta G(\mathbf{s}, \mathrm{pH}) = (\ln 10) k_B T \sum_{i=1}^{N} s_i (\mathrm{pH} - \mathrm{pK}_{a,i}) + E_{el}(\mathbf{s}) - E_{el}(\mathbf{0}) - \sum_{i=1}^{N} [E_{el}^{m(i)}(s_i) - E_{el}^{m(i)}(0)] \quad (1)$$

where $pK_{a,i}$ is the standard pK_a of site i, and $E_{el}(\mathbf{s})$ and $E_{el}(\mathbf{0})$ are the electrostatic free energies of the protein in protonation state **s** and in the fully unprotonated reference state, respectively. $E_{el}^{m(i)}(s_i)$ and $E_{el}^{m(i)}(0)$ are the electrostatic free energies of the model compound for site i in protonation state s_i and in the unprotonated state, respectively. Model compounds are defined as the isolated amino acid residue in solution with neutral termini. We also define the pK_a^{intr} of site i as the standard pK_a (pK_a) of the model compound plus a pK_a shift caused by electrostatic interactions with the protein (backbone, nontitrating residues, titrating residues in their uncharged states) and the desolvation effect.[22]

We calculated all $E_{el}(\mathbf{s})$ values by solving the finite-difference LPB equation using the program UHBD.[18] A dielectric constant of 80 was used for the solvent, and a dielectric constant of 4 or 20 was used for the protein and the model compounds. All calculations were done with an ionic strength of 145 mM, a temperature of 293 K, and a Stern (ion exclusion) layer of 2 Å. Several focusing grids were used to achieve a final grid spacing of 0.25 Å. We used pK_a values of 4.0 for Asp, 4.4 for Glu, 10.46 for Cys, 6.42 for His, 10.13 for Tyr, 12.48 for Arg, 10.79 for Lys, 3.8 for a C-terminal carboxyl, and 7.5 for a N-terminal amino group.[6,45] The change in charge of a residue upon ionization was distributed over several atoms of the sidechain in accord with partial charge assignments in the CHARMM program,[46] as given in Schaefer et al.[11] Atomic radii and partial charges (background atoms) were assigned according to the CHARMM all-hydrogen parameter set 22.[47] Further details of the electrostatic calculations have been given previously.[11]

After determination of the electrostatic free energies $E_{el}(\mathbf{s})$ and $E_{el}^{m(i)}(s_i)$, the average degree of protonation $\langle x_i \rangle$ of site i can be obtained by evaluating a Boltzmann weighted sum over all 2^N charge states **s** of the protein:

$$\langle x_i(\mathrm{pH}) \rangle = \frac{1}{Z(\mathrm{pH})} \sum_{\mathbf{s}} s_i \exp\left[\frac{-\Delta G(\mathbf{s}, \mathrm{pH})}{k_B T}\right], \quad (2)$$

where $\langle\ \rangle$ denotes the average, and Z(pH) is the protonation partition function of the protein.

$$Z(\mathrm{pH}) = \sum_{\mathbf{s}} \exp\left[\frac{-\Delta G(\mathbf{s}, \mathrm{pH})}{k_B T}\right]. \quad (3)$$

The pK_a's are determined by calculating $\langle x_i(\mathrm{pH}) \rangle$ at a series of pH values (interval of 0.1 pH-unit) and finding the pH at which $\langle x_i(\mathrm{pH}) \rangle$ equals 0.5.

For systems with more than 25–30 sites, the evaluation of the partition function and of the average in Equation 2 becomes computationally intractable. For HEWL, which has 32 sites, we therefore made use of a Monte Carlo (MC) program by Beroza et al.[48] The MC method avoids doing the full summation while still being able to achieve very accurate values. At a given pH, the average protonation of the sites was determined by performing 2000 "full MC" steps followed by 4000 "reduced MC" steps, where 1 MC step corresponds to N random attempts to change the protonation state of the system (N is the number of sites plus the number of strongly interacting, coupled sites; for details, see Beroza et al.[48] and Schaefer et al.[11]). Full MC steps are applied to all titrating sites, and reduced MC steps are applied to the subset of titrating sites for which the full MC steps resulted in a value of $\langle x_i(\mathrm{pH}) \rangle$ different from 0 or 1 (fully unprotonated or protonated, respectively) by more than 0.01%.

Averaging Over Trajectory

To account for the conformational flexibility of the protein structure and take account of biases in the crystal conformation, we calculated the pK_a values of an ensemble of protein conformations. This ensemble was created by calculating a molecular dynamics (MD) trajectory of the protein with inclusion of explicit water molecules. We used CHARMM[46]

with the all-hydrogen parameter set 22[47] to set up the systems and calculate the trajectories. The standard protonation states of the residues at pH 7 were used, i.e., the N-terminus, Arg, and Lys were positively charged, the C-terminus, Asp, and Glu were negatively charged, and His residues were neutral with the hydrogen on the $N^{\delta 1}$ atom. The method was applied to bovine pancreatic trypsin inhibitor (BPTI) and hen egg-white lysozyme (HEWL), for which we used the Protein Data Bank crystal structures 4pti[49] and 1lyz[50] as starting structures, respectively. Recently, more accurate HEWL crystal structures have become available (e.g., 1hel[51] and 2lzt[52]), and the use of the relatively old 1lyz structure provides a good test case of the method based on the use of a suboptimal crystal structure.

Hydrogen atoms of the protein and crystal waters were added with the HBUILD facility in CHARMM. The proteins were then solvated in a sphere of equilibrated TIP3 water molecules with a radius of 32 Å and 37 Å for BPTI and HEWL, respectively. The proteins thus had a solvation shell of at least 15 Å around all residues. Waters with their oxygen atom closer than 2.8 Å to a protein or crystal water heavy atom were discarded. A stochastic boundary was added to the system,[53] with a reaction region of radius 29 Å for BPTI and 34 Å for HEWL, and a buffer region shell of 3 Å for both proteins. Stochastic-boundary molecular dynamics propagate atoms within the reaction region according to regular Newtonian dynamics, while atoms in the buffer region are propagated by Langevin dynamics.[54] Outside the buffer region a boundary force is applied that prevents the water molecules from escaping the sphere. With the coordinates of the protein atoms fixed, we did a short (50 steps) minimization of the waters, followed by 10 ps of MD to let the waters relax around the protein. The overlay of the water sphere, minimization, and dynamics procedure was repeated three times, with the TIP3 sphere rotated by 90° around the Cartesian X, Y, and Z axis, respectively. This was done to make sure that no water-sized holes remained in the system. The BPTI system contained 892 protein atoms and 4435 water molecules; for HEWL the corresponding numbers were 1960 and 6665, respectively. To speed up the dynamics calculations, we multiplied the hydrogen masses by a factor of 10, which enabled us to use a timestep of 2.5 fs. The mass-scaling does not affect equilibrium properties of the trajectory and has been shown to improve conformational sampling.[55]

After the addition and equilibration of the waters, the entire system was heated to 300 K by random velocity reassignment and equilibrated for 10 ps. We then performed a 100 ps MD calculation for data collection, and stored the coordinates at 0.25 ps intervals. Two separate ensembles of conformations were derived from the 100 ps trajectories. The first consists of 20 conformations obtained by averaging the atomic coordinates over 5 ps intervals (0–5 ps, 5–10 ps, etc.). The second consists of trajectory snapshots after every 2.5 ps, and includes 40 conformations. The two ensembles are denoted ϵ_{5ps} and ϵ_{snap} in the following.

The averaging procedure for the pK_a calculations was done in three ways: first, at the conformational level, second, at the electrostatic free energy level, and third, at the titration curve level. For the first method, termed C_{ave} in the following, we calculated the average structure of the 100 ps trajectory (using all 400 stored coordinate sets) and then proceeded with the titration calculation as for a single conformer. In the second method, termed E_{ave}, the electrostatic free energies of the protein ($E_{el}(\mathbf{s})$) and the model compounds ($E_{el}^{m(i)}(s_i)$) were arithmetically averaged over the members of the ensemble. It should be noted that the model compound coordinates were defined for each protein conformation, resulting in different values of $E_{el}^{m(i)}(s_i)$ for different ensemble members. This corresponds to the standard method used for single conformations; i.e., the model compound for a given amino acid always has the same conformation as that amino acid in the protein. In this method, we are effectively averaging the $\Delta G(\mathbf{s}, pH)$ values for each protonation state $\mathbf{s}$ over the ensemble of conformations:

$$\langle \Delta G(\mathbf{s},pH)\rangle_\epsilon = \frac{1}{N_\epsilon}\sum_{k=1}^{N_\epsilon} \Delta G_k(\mathbf{s}, pH), \qquad (4)$$

where N_ϵ is the number of conformations in the ensemble ϵ. The averaged $\langle \Delta G(\mathbf{s}, pH)\rangle_\epsilon$ values were subsequently used to calculate the titration curve and pK_a's as for a single conformer. For the third method, termed $Titr_{ave}$, we calculated protein and individual site titration curves for all conformations in the ensemble, and then determined the arithmetic average of the titration curves. If $\langle x_i\rangle_k$ is the titration curve of site i calculated for conformation k in the ensemble ϵ, the average according to the third method is:

$$\langle x_i\rangle_\epsilon = \frac{1}{N_\epsilon}\sum_{k=1}^{N_\epsilon} \langle x_i\rangle_k. \qquad (5)$$

The last averaging procedure ($Titr_{ave}$) is physically most realistic, since it reflects the existence of an ensemble of different conformations that each have their individual protonation states at a particular pH, and the macroscopically measured pK_a's are an average over all members of the ensemble. However, it is computationally the most demanding because it requires N_ϵ calculations of the average protonation of the sites (titration calculations). Thus, if either the C_{ave} method or, to a lesser extent, the E_{ave} method, were to give similar results, it would considerably reduce the required computation time. Moreover, by comparing the three methods, we are able to deter-

mine the origin of the change in the calculated pK_a values relative to those obtained from a single structure. This is not clear from any of the previous studies,[24,41,44] which used only a single method.

The method of Bashford and Gerwert[24] is similar to $Titr_{ave}$. They determined the pK_a's of the individual conformations and then averaged them. Their method is likely to be more sensitive to residues that have non-standard titration curves, and, consequently, unreliable pK_a's, in any one of the conformations. The method used by Zhou and Vijayakumar[44] also corresponds to our $Titr_{ave}$ method. However, in their method, the contribution of the different protonation states of each structure are weighted according to their electrostatic energy relative to that of the protonation state used in the MD simulation. We used all structures obtained from the molecular dynamics trajectories with equal weights for consistency with earlier work and between the averaging methods ($Titr_{ave}$ and E_{ave}) and the use of the average structure from the MD trajectory (C_{ave}). It is the main objective of this study to evaluate the usefulness of the former, computationally more expensive methods, relative to the latter.

RESULTS

BPTI

The root mean square deviation (rmsd) of BPTI from the crystal structure over the 100 ps MD trajectory shows an initial increase over the first 30 ps of the simulation. During the final 70 ps, the mass-weighted rmsd (backbone rmsd) fluctuates around a mean value of 1.4 Å (1.0 Å). Since we are mainly interested in obtaining a set of different conformations from the trajectory, we collected structures from the entire 100 ps simulation.

Table I lists the calculated pK_a values from the crystal structures and the three different trajectory averaging methods (see Methods). Experimentally determined pK_a's[56–58] and values calculated by Yang et al.[34] are also given. As a measure of the accuracy, we calculated the rmsd and the average absolute deviation (aad) of the calculated pK_a's with respect to the experimental data where available (no experimental values are known for Tyr residues). The calculated pK_a's in Table I, including those by Yang et al.[34] for the same crystal structure, were obtained using a protein dielectric constant $\epsilon_i = 4$; their approach was similar to ours except for the fact that Tyr residues were not allowed to titrate; also they used different atomic charges and radii. As pointed out by Antosiewicz et al.,[23] the calculation with $\epsilon_i = 4$ based on the crystal structure (column 4pti) gives results that are significantly worse than the null model where all sites in the protein are assigned their standard pK_a's (column Std): the aad with respect to the experimental pK_a's is 1.06 as compared with 0.59 for the null model. In the calculation based on the crystal structure, the Lys pK_a's are relatively well predicted, which is explained by their high degree of solvent exposure and, as a consequence, their small deviation from the standard pK_a. Asp 3, which has a lowered pK_a compared to its standard pK_a is predicted correctly, but for Asp 50 the pK_a shift is considerably overestimated. The predicted pK_a shift for Glu 7 has the wrong sign, +1 pH-unit, as compared with the experimental pK_a shift of −0.7 pH-units. For the N-terminus, a pK_a decrease is calculated whereas an increase is observed experimentally. The N-terminus is better predicted by Yang et al., though it is not clear why.

The average error of the calculated pK_a's is reduced significantly when the various averaging methods are employed that make use of ensembles of MD-generated conformations. The pK_a shift calculated from the average conformation of the 100 ps trajectory (C_{ave} method) has the correct sign for the Glu 7, which was shifted in the wrong direction when using the crystal structure. The aad for all residues decreases from 0.79 to 0.41, and the aad for the non-Lys residues decreases from 0.87 to 0.42. The C_{ave} method yields pK_a's that agree better with experiment than the null model (0.59).

The second averaging method, E_{ave}, in which site-site interaction energies are averaged over 20 conformations (ensemble ϵ_{5ps}), also leads to significant improvements over the crystal structure calculation. The aad from experimental pK_a's are virtually identical to the C_{ave} method (0.37 vs. 0.41 for all residues, 0.46 vs. 0.42 for non-Lys residues, see Table I). However, the pK_a shift of the N-terminus is predicted in the right direction; the predicted pK_a shift for Asp 50 is overestimated, slightly more so than with the C_{ave} method. Averaging the titration curves (method $Titr_{ave}$) gives virtually identical results to the E_{ave} method (Table I). For this method, we used two different ensembles, ϵ_{5ps} and ϵ_{snap}. There are no significant differences between the results based on the two ensembles. This shows that the differences in averaging, discussed in connection with Eqns. 4 and 5, are not significant.

As indicated by Yang et al.,[34] the overestimation of the pK_a shift of Asp 50 in the crystal structure of BPTI may be caused by the presence of a salt bridge between Asp 50 and Arg 53. In the crystal structure this salt bridge (between Asp 50 $O^{\delta 1}$ and Arg 53 $N^{\eta 2}$ hydrogen) has a length of 2.63 Å. In the averaged structure the closest distance between an O^{δ} and an H^{η} is 3.47 Å, resulting in a weaker effect of Arg 53 on the titration of Asp 50. Figure 1 shows the breaking and forming of this salt bridge along the trajectory, plotted together with the absolute error of the calculated pK_a of Asp 50. The salt bridge that exists in the crystal structure breaks at t ~10 ps, accompanied by a decrease in the error. As the salt bridge forms transiently at 60 ps, this time involving Asp50 $O^{\delta 2}$, there is a sharp increase in the error. After that, there are three instances where the distance O^{δ}-H^{η}

TABLE I. BPTI, Calculated pK_a's for $\epsilon_i = 4$[†]

	Exp	Std	4pti	6pti	ϵ_{5ps}	ϵ_{snap}	E_{ave}	C_{ave}	YA
Nter1	8.1	7.50	5.97	7.48	7.56	7.53	7.55	7.17	7.0
Arg1	—	12.48	12.90	15.34	13.78	13.86	13.50	13.70	—
Asp3	3.4	4.00	3.40	3.43	3.46	3.45	3.45	3.40	3.6
Glu7	3.7	4.40	5.38	4.44	4.32	4.34	4.33	3.97	3.4
Tyr10	—	10.13	11.24	9.53	10.62	10.72	10.62	11.75	—
Lys15	10.6	10.79	10.79	10.34	10.76	10.76	10.74	10.71	10.7
Arg17	—	12.48	12.67	12.68	12.50	12.50	12.49	12.47	—
Arg20	—	12.48	14.81	14.43	13.68	13.58	13.62	13.70	—
Tyr21	—	10.13	11.01	11.04	11.34	11.33	11.34	12.32	—
Tyr23	—	10.13	15.78	12.06	16.90	>20	17.04	18.36	—
Lys26	10.6	10.79	10.78	10.79	10.82	10.82	10.83	10.81	10.8
Tyr35	—	10.13	11.80	10.76	14.62	14.91	14.65	15.83	—
Arg39	—	12.48	12.64	12.91	12.52	12.51	12.51	12.44	—
Lys41	10.8	10.79	10.01	10.92	10.97	10.88	10.96	10.48	10.3
Arg42	—	12.48	12.89	12.71	12.75	12.78	12.76	12.70	—
Lys46	10.6	10.79	10.30	10.31	10.29	10.27	10.29	10.17	10.3
Glu49	3.8	4.40	4.12	3.63	4.10	4.03	4.12	4.09	4.5
Asp50	3.0	4.00	1.49	3.58	2.10	1.89	2.07	2.34	1.7
Arg53	—	12.48	14.87	13.42	13.57	13.63	13.63	13.37	—
Cter58	2.9	3.80	3.73	—[†]	3.31	3.34	3.32	3.77	3.6
rmsd		0.59	1.06	0.41	0.44	0.49	0.45	0.51	0.66
aad		0.50	0.79	0.41	0.37	0.38	0.37	0.41	0.54
rmsd ac.		0.78	1.09	0.48	0.54	0.61	0.56	0.52	0.75
aad ac.		0.76	0.87	0.38	0.46	0.49	0.47	0.42	0.64

[†]Protein dielectric constant $\epsilon_i = 4$. Column labels: Exp, experimental pK_a's;[56–58] Std, standard pK_a's;[6,45,61] 4pti/6pti, protein data bank crystal structures; $\epsilon_{5ps}/\epsilon_{snap}$, averaging titration curves of the ensemble $\epsilon_{5ps}/\epsilon_{snap}$ (see text); E_{ave}, averaging electrostatic free energies E_{ij} over the ϵ_{5ps} ensemble; C_{ave}, pK_a's of the average structure of the MD trajectory; YA, results of Yang et al.[34] Row labels: rmsd/aad, root mean square deviation/average absolute deviation from the experimental pK_a's (ac., for acidic residues Asp, Glu, C-terminus).
[†]Residues 57 and 58 are undefined in 6pti.

rises over 3 Å (at 62, 75, and 90–97 ps), in all cases accompanied by a decrease in the error of the calculated pK_a of Asp 50. The experimental pK_a of Asp 50 is thus indicative of the fact that in solution the salt bridge with Arg 53 is not present.

We used the LPB equation to calculate energies of interaction of the salt bridge and desolvation energies of the salt bridge residues. The electrostatic interaction energy between the negative charge of Asp 50 and the positive charge of Arg 53 was between −2 and −3 kcal/mol when the salt bridge was formed, and between −0.3 and −0.5 when it was absent. Breaking of the salt bridge was always accompanied by an increase in the electrostatic solvation energy from approximately −16.0 kcal/mol to −16.5 kcal/mol for Asp 50, and from approximately −15.0 kcal/mol to −16.5 kcal/mol for Arg 53. Thus, from electrostatic effects alone salt bridge formation is calculated to lead to a free energy change near zero. This is in accord with the fact that during the simulation both configurations contribute.

The experimentally observed pK_a shift of the N-terminus (positive) and the C-terminus (negative) has been explained by the formation of a salt bridge between these sites as observed in NMR experiments.[57] The salt bridge between N-terminus and C-terminus is not observed during the MD simulation; the shortest distance between the N-terminal nitrogen and any of the two C-terminal oxygens is about 5 Å at t = 60 ps, and there is no correlation between this distance and the pK_a error. For comparison, the shortest terminal-nitrogen to C-terminal oxygen distance in the crystal structure is 7.19 Å. The electrostatic interaction energy, calculated with the LPB equation, between the charges of the two residues varied between −0.1 and −0.4 kcal/mol, and only small variations in electrostatic solvation energies of the residues exist between the different conformations, which is consistent with the absence of a salt bridge. Since the calculated pK_a values of the termini do not show the experimentally observed shifts, it is likely that the salt bridge does play a role.

Although other papers have stressed the importance of conformational averaging in pK_a calculations, it appears that the dominant effect of using the conformational ensemble is an improvement in the average structure of the protein. In most cases, the pK_a shifts calculated with the C_{ave} method are similar to the shifts calculated with the E_{ave} and $Titr_{ave}$ methods. Differences on the order of more than one pK_a unit occur only for Tyr residues. This is caused by the large fluctuations in predicted Tyr pK_a's of the different structures from the 100 ps trajectory (re-

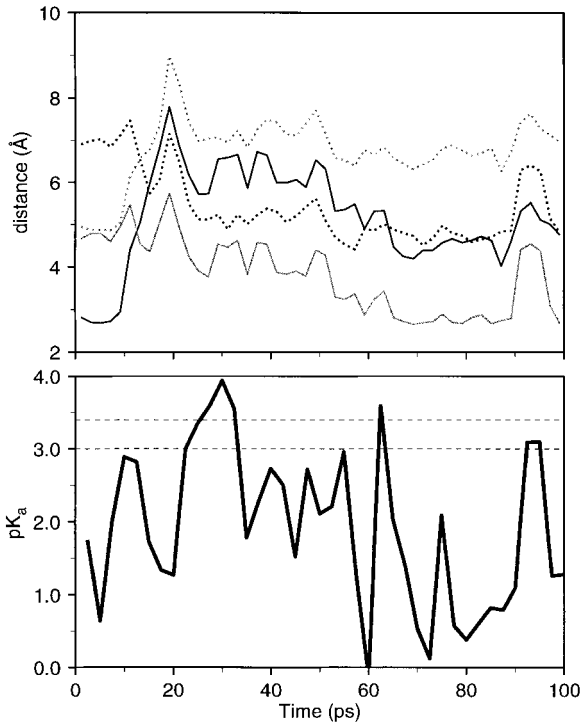

Fig. 1. **Top:** BPTI, distances between the carboxyl oxygens of Asp 50 and the guanidinium nitrogens of Arg 53 during the MD simulation (averages over 2 ps intervals). Black line: $O^{\delta 1} \ldots N^{\eta 2}$; gray line: $O^{\delta 2} \ldots N^{\eta 2}$; black dots: $O^{\delta 2} \ldots N^{\eta 1}$; gray dots: $O^{\delta 1} \ldots N^{\eta 1}$. **Bottom:** BPTI, calculated pK_a of Asp 50 for structures every 5 ps from the MD trajectory. Protein dielectric constant ϵ_i = 4. The experimental pK_a-range (3.0 to 3.4) is indicated by the horizontal lines.[58]

sults not shown). The fluctuations are correlated to solvent accessibilities of the Tyr hydroxyl groups.

The calculated pK_a values based on the crystal structures 5pti (not shown in Table I) and 6pti are significantly better than the calculations based on 4pti, most notably for the N-terminus, Glu 7, and Asp 50. The results for Asp 50 are in agreement with the correlation between the Asp 50–Arg 53 distance and the error in the pK_a value (Fig. 1); the $O^{\delta 1}$ to $N^{\eta 2}$ distances in 5pti and 6pti are 3.6 Å.

In agreement with results obtained previously,[11,23,36] the use of a protein dielectric constant ϵ_i of 20 improves the results significantly (Table II). Even the titration curve obtained from the crystal structure, i.e., without conformational averaging, has slightly smaller errors than the one obtained from averaging titration curves with an ϵ_i of 4 (Table I). Averaging over titration curves or using the MD averaged structure (C_{ave}) with an ϵ_i of 20 further improves the results. A plot of the aad between calculated and experimental pK_a's for different conformations shows that the conformational variability has a small effect on the results with an ϵ_i of 20, in contrast to the results with an ϵ_i of 4 (Figure 2).

Hen Egg-White Lysozyme

Since we did not see significant differences in predicted pK_a's between averages over the ϵ_{5ps} and ϵ_{snap} ensembles for BPTI, we calculated average titration curves for HEWL only with the ϵ_{5ps} ensemble. The rmsd of HEWL from the crystal structure over the 100 ps MD trajectory fluctuated between 0.81 and 1.08 Å for the backbone atoms. Table III lists the results obtained for the E_{ave} and $Titr_{ave}$ (column ϵ_{5ps}) averaging procedures and for two crystal structures, with a protein dielectric constant ϵ_i of 4. The calculated deviations from the experimental pK_a's include Tyr residues. The inclusion of Tyr in the pK_a calculations may be problematic, since most Tyr residues are buried and their ionization is likely to cause large conformational changes.[20,22]

A comparison between the 1lyz tetragonal crystal structure results with an ϵ_i of 4 (column 1lyz) and those of the $Titr_{ave}$ method (column ϵ_{5ps}) shows that only a relatively small improvement is achieved. The improvement (a reduction of the aad by 29%) is significant but not as important as that for BPTI (reduction of the aad by 53%; Table I). The main reason for this relatively small improvement is the poor predictions for Tyr 53 and Asp 66. When these two residues are excluded from the aad, the improvement is considerably greater (45%). For Tyr 53, none of the averaging methods (for $\epsilon_i = 4$) yields a predicted pK_a of less than 20. The conformational variability that is accounted for in the present set of MD conformations is, therefore, insufficient to reduce the anomalously high predicted pK_a shift of Tyr 53. The main cause for this large error is the interaction between Tyr 53 and Asp 66, whose pK_a is also predicted poorly. This is confirmed by considering the pK_a^{intr} values for Tyr 53, which accounts for the interaction of the site with the solvent and the polar atom groups of the protein, but not for the interaction with other titratable groups. Figure 3 shows that the pK_a^{intr} of Tyr 53 fluctuates around the experimental value of 12.1. When using a protein dielectric constant of 4, the calculated pK_a of Tyr 53 is larger than 20 for all conformations except the last, whereas the pK_a of Asp 66 is extremely small (<-4). These large pK_a shifts are caused by the strong interaction between the two residues (average distance Tyr53 O^{η} to Asp66 $O^{\delta 1}$ = 2.75 Å). In the crystal structure this distance is larger (3.02 Å); this yields a calculated pK_a of Asp 66 that is closer to the experimental value. When ϵ_i is set to 20 (Table IV), the interaction between Tyr 53 and Asp 66 is reduced and the calculated pK_a's agree very well with experiment. The interaction energy between the unprotonated Asp 66 and the protonated Tyr 53 in the crystal structure 1lyz equals −3.4 kcal/mol for $\epsilon_i = 4$, and is reduced to −0.65 kcal/mol for $\epsilon_i = 20$.

Glu 7 and Glu 35 are the two other residues whose calculated pK_a's agree better with experiment when

TABLE II. BPTI, Calculated pK_a's for $\epsilon_i = 20$[†]

	Exp	Std	4pti	ϵ_{5ps}	ϵ_{snap}	E_{ave}	C_{ave}	AN[a]
Nter1	8.1	7.50	7.11	7.63	7.63	7.63	7.56	7.1
Arg1	—	12.48	14.21	14.34	14.35	14.35	14.43	—
Asp3	3.4	4.00	3.45	3.45	3.46	3.47	3.41	3.4
Glu 7	3.7	4.40	3.59	3.76	3.76	3.76	3.72	3.7
Tyr 10	—	10.13	9.82	9.69	9.69	9.68	9.79	—
Lys 15	10.6	10.79	10.91	10.80	10.79	10.80	10.78	10.5
Arg 17	—	12.48	12.61	12.54	12.54	12.55	12.53	—
Arg 20	—	12.48	13.61	13.57	13.56	13.57	13.64	—
Tyr21	—	10.13	10.30	10.43	10.44	10.41	10.56	—
Tyr23	—	10.13	10.84	10.93	10.90	10.93	11.05	—
Lys26	10.6	10.79	10.87	10.87	10.87	10.88	10.88	10.5
Tyr35	—	10.13	9.45	9.92	9.97	9.91	10.10	—
Arg39	—	12.48	12.72	12.70	12.69	12.69	12.68	—
Lys41	10.8	10.79	11.19	11.32	11.31	11.33	11.24	10.8
Arg42	—	12.48	12.79	12.79	12.80	12.79	12.77	—
Lys46	10.6	10.79	10.63	10.59	10.57	10.58	10.52	10.2
Glu49	3.8	4.40	3.97	4.06	4.05	4.05	4.08	3.9
Asp50	3.0	4.00	2.46	2.75	2.70	2.75	2.78	2.7
Arg53	—	12.48	13.64	13.28	13.30	13.29	13.26	—
Cter58	2.9	3.80	3.50	3.41	3.42	3.42	3.50	3.5
rmsd		0.59	0.45	0.32	0.32	0.32	0.33	0.40
aad		0.50	0.35	0.26	0.27	0.27	0.27	0.26
rmsd ac.		0.78	0.37	0.28	0.29	0.28	0.31	0.30
aad ac.		0.76	0.29	0.23	0.24	0.23	0.23	0.20

[†]Protein dielectric constant $\epsilon_i = 20$. Column/row labels are the same as in Table I.
[a]Results of Antosiewicz et al.[23]

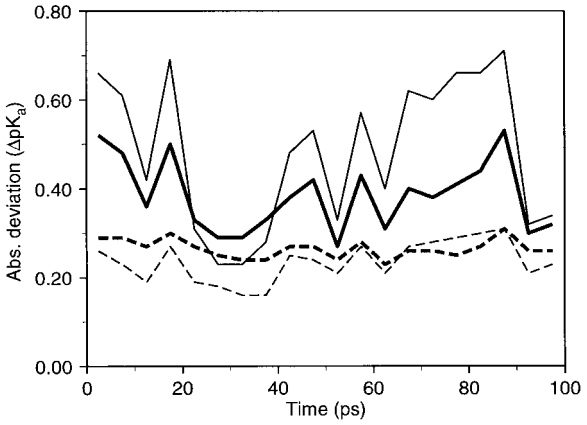

Fig. 2. BPTI, average absolute deviation between calculated and experimental pK_a's for conformations averaged over 5 ps intervals of the MD trajectory (ensemble ϵ_{5ps}). Thick lines: all titratable sites; thin lines: Asp, Glu, and C-terminus. Solid lines: protein dielectric constant $\epsilon_i = 4$; dashed lines: $\epsilon_i = 20$.

using the crystal structure, rather than the ensemble averages (for $\epsilon_i = 4$). For Glu 7 ($pK_a^{exp} = 2.85$), use of the crystal structure yields a pK_a of 2.36, whereas averaging the titration curves over the ϵ_{5ps} ensemble leads to a predicted pK_a of 0.27. Interestingly, Yang and Honig[22] observed an increase of the predicted pK_a when the MD averaged structure was used. This is explained by the fact that in their MD simulation the salt bridge between Glu7 and Lys 1 did not persist, whereas in our simulation it became stronger (the average distance of the N^{ζ} atom of Lys 1 to $O^{\epsilon 1}$ and $O^{\epsilon 2}$ of Glu 7 decreased from 3.4 Å in the crystal structure to 3.35 Å in the MD averaged structure).

One way of analyzing the titration behavior of proteins is to consider intrinsic pK_a's and the contributions to their values: the solvation (Born) energy in the protein and the interaction with the background charges (polar atom groups) in the protein, both relative to the same energy term in the isolated amino acid (model compound). Table V lists the desolvation and background charge effects for Glu 7 and 35, and for Asp 52, 101, and 119. The change in the solvation and background charge energies between model compound and protein is expressed in terms of pK_a shifts, $\Delta pK_a = \Delta G/(\ln 10\ RT)$, where ($\ln 10\ RT$) = 1.37 kcal/mol at T = 293 K. In the MD averaged conformation the desolvation pK_a shift of Glu 7 is slightly smaller than in the crystal structure, but the background energy has changed markedly from favoring protonation ($\Delta pK_a = 0.69$) to favoring deprotonation ($\Delta pK_a = -1.82$). This results from the fact that during the MD simulation, interactions of Asp and Glu residues with polar atom groups are strengthened because the ionized charge state is used. Consistently, the background charge ΔpK_a's of Glu and Asp in the MD averaged structure are negative, whereas in the crystal structure they are negative for only one out of five acidic residues (Table V). For Glu 35 ($pK_a^{exp} = 6.2$), the calculated value

TABLE III. HEWL, Calculated pK_a's for $\epsilon_i = 4$[†]

	Exp	Std	1lyz	2lzt	ϵ_{5ps}	E_{ave}	C_{ave}	BA	YA	YO
Nter1	7.90	7.50	8.62	8.40	7.52	7.51	7.09	5.00	6.90	7.86
Lys1	10.80	10.79	16.59	9.94	12.51	12.51	12.28	10.80	10.90	11.13
Arg5	—	12.48	15.10	14.18	14.16	14.17	14.25	—	—	—
Glu7	2.85	4.40	2.36	2.74	0.27	0.31	1.31	1.20	4.10	2.62
Lys13	10.50	10.79	13.96	10.99	11.75	11.75	11.62	10.10	10.80	11.20
Arg14	—	12.48	13.16	12.61	12.80	12.81	12.73	—	—	—
His15	5.36	6.42	4.60	5.02	4.56	4.54	4.71	2.40	5.60	6.16
Asp18	2.66	4.00	1.98	1.46	3.27	3.23	3.56	2.60	2.20	2.68
Tyr20	10.30	10.13	12.60	17.93	11.41	11.50	11.55	12.10	10.30	12.87
Arg21	—	12.48	13.69	12.66	13.40	13.46	13.38	—	—	—
Tyr23	9.80	10.13	10.63	11.03	10.94	10.89	11.04	10.10	9.80	10.34
Lys33	10.60	10.79	10.30	10.73	10.66	10.80	10.57	7.70	10.60	10.90
Glu35	6.20	4.40	6.34	5.23	4.95	4.93	4.91	6.20	3.80	4.21
Arg45	—	12.48	10.11	12.51	12.32	12.25	12.29	—	—	—
Asp48	1.60	4.00	4.72	−1.07	0.08	0.06	0.10	1.60	1.70	3.95
Asp52	3.68	4.00	8.81	2.49	2.58	2.55	3.24	8.50	4.20	6.79
Tyr53	12.10	10.13	>20	>20	>20	>20	>20	18.80	12.10	18.60
Arg61	—	12.48	12.70	14.87	12.76	12.83	12.59	—	—	—
Asp66	0.90	4.00	−1.71	−0.99	−4.73	−4.75	−4.80	2.20	−1.00	1.95
Arg68	—	12.48	15.42	15.17	14.14	14.14	14.23	—	—	—
Arg73	—	12.48	11.67	12.45	12.15	12.11	12.19	—	—	—
Asp87	2.07	4.00	1.22	0.96	0.83	0.83	1.19	0.80	2.10	2.77
Lys96	10.80	10.79	10.20	12.79	11.13	10.99	10.62	8.90	10.70	9.73
Lys97	10.30	10.79	10.77	11.13	11.06	11.12	10.73	8.40	10.70	11.01
Asp101	4.09	4.00	9.81	4.75	3.07	3.08	3.03	4.30	2.30	4.89
Arg112	—	12.48	13.32	12.71	13.38	13.42	13.45	—	—	—
Arg114	—	12.48	13.26	13.19	13.31	13.31	13.40	—	—	—
Lys116	10.40	10.79	9.97	9.21	11.65	11.76	11.62	9.70	10.80	9.40
Asp119	3.20	4.00	−0.09	3.70	3.31	3.26	3.47	1.30	3.60	3.39
Arg125	—	12.48	17.07	13.57	12.78	12.85	12.71	—	—	—
Arg128	—	12.48	12.35	12.64	12.44	12.43	12.48	—	—	—
Cter129	2.75	3.80	−0.01	2.68	0.08	0.09	0.23	2.20	3.10	2.50
rmsd		1.28	3.17	2.64	2.45	2.45	2.39	2.34	0.95	1.89
aad		0.94	2.30	1.59	1.64	1.65	1.54	1.63	0.65	1.20
rmsd ac.		1.64	2.95	1.23	2.22	2.22	2.10	1.95	1.17	1.42
aad ac.		1.40	2.32	0.97	1.68	1.68	1.52	1.34	0.86	1.04
rmsd-1		1.04	2.73	2.05	1.30	1.30	1.15	1.90	0.87	1.28
aad-1		0.77	1.99	1.25	1.10	1.11	0.99	1.38	0.58	0.93

[†]Protein dielectric constant $\epsilon_i = 4$. Column/row labels are the same as in Table I, except for: Exp, experimental pK_a's;[59,60] 1lyz/2lzt, tetragonal/triclinic crystal structure; BA, results of Bashford and Karplus[20] using the 1lyz crystal structure; YA, results of Yang and Honig[22] using the average conformation from a 5 ps MD trajectory; YO, results of You and Bashford[41] using a minimized 1lzt crystal structure; rmsd/aad ac., error for acidic sites including His; rmsd-1/aad-1, error for all sites except Tyr53 and Asp66.

based on the trajectory averaging methods (in the range 4.91 to 4.95) is also significantly worse than the one based on the crystal structure (6.34, see Table III). This is largely caused by a reduction in the desolvation effect (Table V); i.e., during the MD simulation, the solvation of Glu 35 in the protein is significantly improved relative to that in the crystal structure.

Use of the trajectory averaging methods leads to significant improvements in calculated pK_a values for Asp 52, 101, and 119, as compared with the calculation based on the crystal structure. Asp 52 is not predicted well using the crystal structure because the large desolvation effect on its pK_a is not compensated by the background charge effect (Table V). By contrast, the background charge effect more than offsets the desolvation effect in the MD averaged structure. This leads to a pK_a^{intr} of 3.31, which is close to the experimental pK_a of 3.68. Asp 101, whose experimental pK_a is close to the standard pK_a of 4, has a very high predicted pK_a (9.81) in the crystal structure due to a large and positive desolvation and background charge pK_a shifts. In the MD averaged structure, the solvation and background pK_a shifts are small and have opposite signs, resulting in a predicted pK_a that is much closer to the experimental value. The large deviation of the pK_a of Asp 101 in the crystal structure is caused by an unrealistically close contact between the $O^{\delta 1}$ of Asp 101 and the backbone carbonyl oxygen of Lys 97 (1.6 Å). In the MD averaged structure this distance is 4.9 Å. Compensation between ΔpK_a(Born) and ΔpK_a-

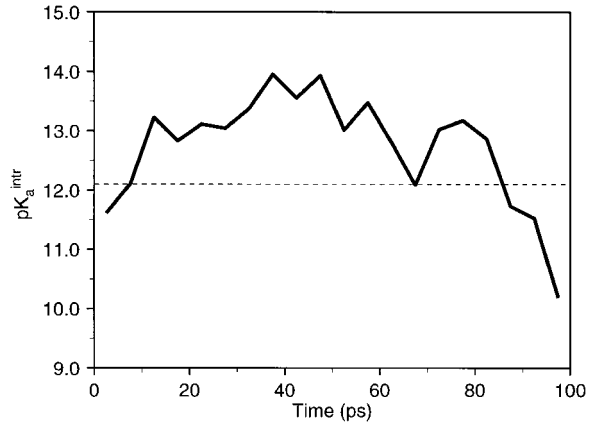

Fig. 3. HEWL, intrinsic pK_a of Tyr 53 for conformations averaged over 5 ps intervals of the MD trajectory (ensemble ϵ_{5ps}). Protein dielectric constant $\epsilon_i = 4$; the experimental $pK_a = 12.1$ is indicated by the horizontal line.

(back) for the C_{ave} method is also seen for Asp 119. However, the main reason for the poor agreement between calculated and experimental pK_a of Asp 119 in the tetragonal crystal structure is the fact that this residue forms a salt bridge with Arg 125. The favorable interaction in the ionic state of Asp 119 leads to a low calculated pK_a for this site (−0.09, whereas the pK_a^{intr} is 6.42). In both the triclinic crystal structure and the MD averaged structure, the salt bridge with Arg 125 is broken, and the calculated pK_a of Asp 119 agrees much better with experiment. A similar analysis of the difference between tetragonal (1lyz) and triclinic (2lzt) crystal structures has been given by Yang and Honig.[22]

In agreement with the results on BPTI, all trajectory averaging methods work equally well (cf. columns ϵ_{5ps}, E_{ave}, and C_{ave} in Table III). For HEWL, the best results are obtained with the C_{ave} method, although the differences are small. In accordance with results published earlier,[22,23,32] the triclinic crystal structure (2lzt) results in better predicted pK_a's than the tetragonal structure (1lyz). The use of another tetragonal crystal structure (protein data bank identifier 1hel), also leads to improvement over the 1lyz structure, although to a lesser extent when compared with 2lzt (rmsd = 2.95 and aad = 1.97 pH-units for 1hel; not shown in Table III).

A qualitative measure of the accuracy of the pK_a calculation methods is to count the titratable sites for which the pK_a shift $\Delta pK_a = pK_a - pK_a^{std}$ has the same sign as the experimental pK_a shift. For all Asp and Glu residues except Asp 52 and 101, and for His 15 and Tyr 53, significant experimental pK_a shifts are observed (Table III). The calculation based on the 1lyz crystal structure predicts pK_a shifts with the wrong sign for Asp 48 and 101. Using the 1hel crystal structure, all significant pK_a shifts are predicted with the correct sign (not shown in Table III). However, for 1lyz and 1hel the calculated pK_a of Asp 52 differs significantly (by 5.13 and 3.38 pH-units, respectively) from the experimental pK_a. For the 2lzt crystal structure, all pK_a shifts have the correct sign and the pK_a of Asp 52 differs by only 1.19 pH-units from experiment. The trajectory averaging methods lead to a correct sign for the pK_a shifts that are predicted wrongly using 1lyz. Moreover, trajectory averaging reduces the error in the calculated pK_a of Asp 52 from 5.13 to 1.10 pH-units.

Yang and Honig[22] also observed improvements in pK_a predictions when an MD averaged structure was used (column YA in Table III), although to a lesser extent because their results for the 1lyz crystal structure are better than the ones reported here. Since we used the same accessible surface definition and ion exclusion radii as Yang and Honig, the discrepancy between the calculated pK_a's of 1lyz is likely to result from differences in the atomic charge and radius parameters. In particular, the atomic radii of most atoms are larger in this work than in Yang and Honig[22] (e.g., carbon 2.0–2.27 Å vs. 1.9 Å, nitrogen 1.85 Å vs. 1.65 Å). Since larger atomic radii cause weaker solvent screening of site-site interactions, the atomic parameters used in this work are expected to lead to larger pK_a shifts than the parameters used by Yang and Honig. As a test, we calculated the titration curves for the 1lyz crystal structure and the MD averaged structure with the atomic radii of Yang and Honig. In agreement with expectation, this improved the average absolute deviation from the experimental values (aad) of the Asp, Glu, His, and C-terminus pK_a's from 2.32 to 1.90 (crystal structure), and from 1.52 to 1.15 (MD averaged structure). The aad for the crystal structure is close to the one reported by Yang and Honig (1.85). However, their aad value for the MD averaged structure is 0.86, significantly lower than what we find. This discrepancy may be due to differences between the MD trajectories that were used for the averaging, and due to differences in the atomic partial charges.

The use of an ϵ_i of 20 improves calculated pK_a values in all cases. On average, the error in the calculated pK_a's is reduced by 67%. Table IV lists the calculated pK_a's of non-Arg residues in HEWL for $\epsilon_i = 20$. Of the different averaging methods, the pK_a's of the C_{ave} method have the lowest aad from the experimental data (0.70 for all residues). The pK_a shifts of the acidic residues are in the right direction by the correct amount, except for Glu 35. This residue's experimental positive pK_a shift can be explained by desolvation in the protein [ΔpK_a(Born) = 4.44 with $\epsilon_i = 4$], which favors the protonated state. From Table III, the correct shift is predicted using the 1lyz crystal structure with an ϵ_i of 4. When $\epsilon_i = 20$ is used or trajectory averaging is done, this residue becomes better solvated, thus shifting the calculated pK_a to a smaller value.

Figure 4 shows the average error of the calculated pK_a's of HEWL for the ϵ_{5ps} conformations along the

TABLE IV. HEWL, Calculated pK_a's for $\epsilon_i = 20$[†]

	Exp	Std	1lyz	2lzt	ϵ_{5ps}	E_{ave}	C_{ave}	AN[a]
Nter1	7.90	7.50	7.85	7.48	7.54	7.55	7.47	7.90
Lys1	10.80	10.79	12.70	10.53	11.69	11.68	11.64	10.80
Arg5	—	12.48	13.25	13.38	13.10	13.09	13.10	—
Glu7	2.85	4.40	2.84	3.05	2.34	2.32	2.53	3.00
Lys13	10.50	10.79	12.22	11.13	11.43	11.43	11.38	11.40
Arg14	—	12.48	13.10	12.79	12.87	12.88	12.87	—
His15	5.36	6.42	5.72	5.76	5.91	5.92	5.95	4.80
Asp18	2.66	4.00	2.55	2.61	3.19	3.19	3.25	3.00
Tyr20	10.30	10.13	10.20	11.10	9.90	9.91	9.90	9.60
Arg21	—	12.48	13.51	13.67	13.36	13.36	13.32	—
Tyr23	9.80	10.13	9.70	9.99	9.92	9.92	9.93	9.40
Lys33	10.60	10.79	10.55	10.78	10.72	10.72	10.66	10.20
Glu35	6.20	4.40	4.37	4.26	4.27	4.27	4.25	4.40
Arg45	—	12.48	12.06	13.11	12.76	12.76	12.76	—
Asp48	1.60	4.00	3.39	2.10	2.32	2.32	2.31	3.30
Asp52	3.68	4.00	4.80	3.34	3.27	3.26	3.40	5.20
Tyr53	12.10	10.13	12.42	12.92	12.04	12.04	12.00	11.20
Arg61	—	12.48	13.11	13.76	12.89	12.90	12.84	—
Asp66	0.90	4.00	1.68	1.80	1.08	1.11	1.10	2.80
Arg68	—	12.48	14.23	14.78	14.37	14.40	14.42	—
Arg73	—	12.48	12.45	12.72	12.56	12.52	12.54	—
Asp87	2.07	4.00	2.31	2.07	2.28	2.26	2.35	2.90
Lys96	10.80	10.79	11.37	11.85	11.56	11.56	11.51	10.90
Lys97	10.30	10.79	11.12	11.32	11.09	11.09	11.02	10.80
Asp101	4.09	4.00	4.50	3.53	3.27	3.29	3.28	4.30
Arg112	—	12.48	13.34	12.98	13.25	13.27	13.25	—
Arg114	—	12.48	12.99	12.86	12.99	13.01	13.02	—
Lys116	10.40	10.79	10.79	10.41	11.23	11.21	11.20	10.40
Asp119	3.20	4.00	2.18	3.06	3.29	3.31	3.34	3.20
Arg125	—	12.48	14.03	13.15	12.78	12.78	12.74	—
Arg128	—	12.48	12.48	12.65	12.55	12.56	12.55	—
Cter129	2.75	3.80	1.97	2.82	1.93	1.94	1.94	2.00
rmsd		1.28	0.93	0.68	0.71	0.71	0.70	0.93
aad		0.94	0.69	0.50	0.57	0.57	0.56	0.72
rmsd ac.		1.64	0.97	0.71	0.78	0.78	0.78	1.17
aad ac.		1.40	0.77	0.46	0.62	0.62	0.61	0.98
rmsd-1		1.04	0.96	0.66	0.74	0.74	0.73	0.84
aad-1		0.77	0.70	0.46	0.62	0.62	0.60	0.64

[†]Protein dielectric constant $\epsilon_i = 20$. Column/row labels are the same as in Table III.
[a]Results of Antosiewicz et al.[23] using the 1lyz crystal structure.

TABLE V. HEWL, Intrinsic pK_a's of Acidic Sites[†]

	1lyz			C_{ave}		
	Born	back	pK_a^{intr}	Born	back	pK_a^{intr}
Glu7	2.95	0.69	8.04	2.27	−1.82	4.85
Glu35	4.44	−1.54	7.29	1.65	−1.26	4.79
Asp52	3.37	0.27	7.64	2.93	−3.62	3.31
Asp101	3.27	3.05	10.32	0.49	−0.82	3.67
Asp119	1.69	0.73	6.42	0.74	−0.47	4.27

[†]Protein dielectric constant $\epsilon_i = 4$. 1lyz, tetragonal crystal structure; C_{ave}, average conformation of the MD trajectory. Column labels: Born/back, pK_a-shift due to the desolvation effect/due to the interaction with the background atoms; pK_a^{intr}, intrinsic pK_a ($pK_a^{intr} = pK_a^{std} + \Delta pK_a^{Born} + \Delta\, pK_a^{back}$).

trajectory. As for BPTI, differences between the conformations lead to significant fluctuations in the average error when a protein dielectric constant $\epsilon_i = 4$ is used, whereas the error for $\epsilon_i = 20$ is nearly constant. In contrast to BPTI, however, the error for $\epsilon_i = 4$ is always significantly larger than the error for $\epsilon_i = 20$. This implies that for $\epsilon_i = 4$, the effect of conformational variability on the pK_a's of at least some of the sites in HEWL cannot be accounted for by averaging over the calculated MD trajectory.

For comparison with the assignment of charges as a function of the protonation state used in this study (see Schaefer et al.[11]), we calculated the pK_a's of HEWL using the charge assignment proposed by Oberoi and Allewell.[32] In their method, a unit charge is assigned to the most solvent exposed atom of the site upon ionization, instead of the assignment of partial charges where the net ±1 charge of the site is distributed among several atoms. In addition, we tested a new scheme in which the net charge was divided over the atoms proportionally to their solvent accessible surface. The atoms over which the unit charge was divided were the carboxyl oxygens

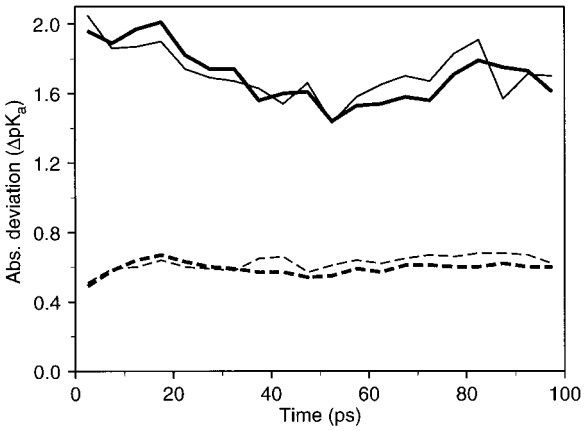

Fig. 4. HEWL, average absolute deviation between calculated and experimental pK$_a$'s for conformations averaged over 5 ps intervals of the MD trajectory (ensemble ϵ_{5ps}). Thick lines: all titratable sites; thin lines: His, Asp, Glu, and C-terminus. Solid lines: protein dielectric constant $\epsilon_i = 4$; dashed lines: $\epsilon_i = 20$.

in Asp, Glu, C-terminus, and $N^{\eta 1}$ and $N^{\eta 2}$ in Arg. The calculated pK$_a$'s of HEWL for these charge assignment methods, using $\epsilon_i = 4$ and $\epsilon_i = 20$, are listed in Table VI. Compared with the results reported in Tables III and IV, the method of Oberoi and Allewell does not lead to a reduction of the error, whereas the proportional charge assignment method leads to a minor reduction of the average error by 2% ($\epsilon_i = 4$) and 3% ($\epsilon_i = 20$).

TABLE VI. HEWL, pK$_a$'s Calculated Using the Charge Distribution Method of Oberoi and Allewell[†]

	Exp	ob1–4	ob2–4	ob1–20	ob2–20
Nter1	7.90	8.56	8.59	7.84	7.83
Lys1	10.80	12.20	16.32	11.55	12.62
Glu7	2.85	6.17	2.53	3.85	2.89
Lys13	10.50	18.05	14.61	13.65	12.44
His15	5.36	3.39	4.48	5.28	5.64
Asp18	2.66	4.84	2.02	3.26	2.61
Tyr20	10.30	12.76	12.59	9.91	10.20
Tyr23	9.80	11.19	10.68	9.94	9.72
Lys33	10.60	10.48	10.29	10.57	10.55
Glu35	6.20	14.55	7.79	5.60	4.58
Asp48	1.60	7.72	5.75	4.20	3.76
Asp52	3.68	7.84	8.27	4.77	4.76
Tyr53	12.10	>20	>20	14.26	12.76
Asp66	0.90	0.57	−1.68	1.66	1.59
Asp87	2.07	2.93	1.24	2.55	2.27
Lys96	10.80	10.19	10.25	11.40	11.42
Lys97	10.30	10.69	10.83	10.98	11.08
Asp101	4.09	8.69	9.43	4.05	4.40
Lys116	10.40	10.48	9.97	10.80	10.81
Asp119	3.20	2.43	3.01	2.96	3.04
Cter129	2.75	−1.15	−0.25	1.47	1.86
rmsd		3.86	3.12	1.16	0.94
aad		2.82	2.25	0.82	0.67
rmsd ac.		4.07	2.81	1.05	0.95
aad ac.		3.32	2.19	0.80	0.68
rmsd-1		3.63	2.67	1.11	0.97
aad-1		2.68	1.94	0.75	0.67

[†]Tetragonal crystal structure (1lyz) used. Column/row labels: Exp/rmsd/aad, same as in Table III; ob1–4 (ob1–20), method of Oberoi and Allewell[32] using a protein dielectric constant $\epsilon_i = 4$ ($\epsilon_i = 20$); ob2–4 (ob2–20), modified method where charges are assigned proportional to the solvent accessible surface of the titrating groups (see text), using $\epsilon_i = 4$ ($\epsilon_i = 20$).

DISCUSSION

The objective of this study was to evaluate the importance of incorporating conformational flexibility into titration curve calculations. We used conformational ensembles produced by a molecular dynamics trajectory, and three different methods for averaging over these trajectories. For both BPTI and HEWL, all averaging methods resulted in increased accuracy of the titration curves, as measured by the deviation from experimental pK$_a$'s of the individual titratable residues (Tables I, II, III, and IV). We found that the dominant effect in the increased accuracy is not due to the use of an ensemble of conformations, but to the generation of a more appropriate structure than the crystal structure. This conclusion is based on the fact that the calculated titration curve of the MD-averaged structure was as accurate as the titration curve obtained as the average of that for the individual members of the ensemble. Large relative improvements of the titration curves versus the crystal structure titration curves were seen for calculations with a protein dielectric constant $\epsilon_i = 4$, and smaller but significant improvements were seen for $\epsilon_i = 20$. For BPTI, the improvements in aad from experimental values, using the C_{ave} method, were 48% and 23%, for an ϵ_i of 4 and 20, respectively. For HEWL, the improvements were 33% and 19%. For HEWL, the improvement with $\epsilon_i = 4$ is significantly greater (50%) when the residues Tyr 53 and Asp 66 are omitted from the average. The proximity of these two residues in the 1lyz crystal structure results in strong charge-charge interactions which are the reason for the poorly predicted pK$_a$'s in the crystal structure. During the MD calculation performed in this study, this distance decreases even more, thus increasing the interaction and the deviation from the experimental pK$_a$'s. One reason for this could be that the simulation was too short and no conformations in the ensemble of structures had a larger Tyr 53–Asp 66 distance, which would result in better predicted pK$_a$'s. The sidechain conformational sampling method used by You and Bashford[41] improved the pK$_a$ values for Tyr 53 and Asp 66 somewhat (from 18.60 and 1.95 to 17.07 and 2.65 for their best method), but they are still significantly worse than the results obtained with an ϵ_i of 20 (Table IV).

Compared to the results of You and Bashford,[41] we obtained comparable relative improvements of calculated pK$_a$ values when conformational variability was introduced by means of MD simulation. For

HEWL they find a 29% improvement in rmsd of predicted vs. experimental pK_a's for all residues. We find a 23% improvement, although it should be noted that their rmsd using the crystal structure structure is lower than ours (2.36 vs. 3.17). It is evident that certain structural features in the crystal structure that give rise to inaccurate pK_a calculations are removed when using an average MD conformation. The application of this method to other proteins is necessary to confirm this hypothesis. Both our method and the one described by You and Bashford[41] reduce the dependency of the results on the protein crystal structure by taking flexibility explicitly into account. An advantage of our method over You and Bashford's is that it can be used with the existing pK_a calculation methods. One only has to generate an MD trajectory of the protein of interest, which is now very straightforward.

Charge assignments based on atom accessibilities did not improve the calculated pK_a values, in contrast to results reported by Oberoi and Allewell[32] (Table VI). As already pointed out by Antosiewicz et al.,[23] such a charge assignment method is somewhat unphysical and thus introduces undefined errors into the methodology.

In conclusion, we believe that the method based on using an average protein structure from a physically realistic MD simulation will generally improve pK_a predictions compared to the use of a single crystal structure. Averaging titration curves of the ensemble members also improves results, but is not better than using the average structure and is computationally more intensive. For cases where very large fluctuations occur, averaging titration curves may be more important. Also, inclusion of different protonation states in the dynamics could improve the sampling. The improvements are significant, although not large enough yet to give results with an ϵ_i of 4 that are as good as those with an ϵ_i of 20. An advantage of this method compared to the one of You and Bashford[41] is that correlated motions of the residues are accounted for by the MD simulation. It is expected that the inclusion of conformers from a longer trajectory would further improve results, because of a better sampling of conformation space.

ACKNOWLEDGMENT

This work was partly supported by a grant from the National Institutes of Health. M. S. is currently supported by a research training grant within the Biotechnology programme of the European Community.

REFERENCES

1. Perutz, M. Electrostatic effects in proteins. Science 201: 1187–1191, 1978.
2. Warshel, A., Russell, S. Calculation of electrostatic interactions in biological systems and in solution. Q. Rev. Biophys. 17:283–422, 1984.
3. Matthew, J.B. Electrostatic effects in proteins. Annu. Rev. Biophys. Biophys. Chem. 14:387–417, 1985.
4. Sharp, K.A., Honig, B. Electrostatic interactions in macromolecules: Theory and experiment. Annu. Rev. Biophys. Biophys. Chem. 19:301–332, 1990.
5. Warshel, A., Åqvist, J. Electrostatic energy and macromolecular function. Annu. Rev. Biophys. Biophys. Chem. 20:267–298, 1991.
6. Fersht, A. Enzyme Structure and Mechanism. W.H. Freeman and Company, New York, 1985:155–175.
7. Szabo, A., Karplus, M. A mathematical model for structure-function relations in hemoglobin. J. Mol. Biol. 72:163–172, 1972.
8. Privalov, P.L. Stability of proteins. Small globular proteins. Adv. Protein Chem. 33:167–241, 1979.
9. Baldwin, R.L., Eisenberg, D. Protein stability. In: "Protein Engineering." Oxender, D., Fox, C.F. (eds.). New York: Alan R. Liss, Inc., 1987:127–148.
10. Yang, A., Honig, B. Electrostatic effects on protein stability. Curr. Opin. Struct. Biol. 2:40–45, 1992.
11. Schaefer, M., Sommer, M., Karplus, M. pH-dependence of protein stability: Absolute electrostatic free energy differences between conformations. J. Phys. Chem. B 101:1663–1683, 1997.
12. Linderstrøm-Lang, K. On the ionisation of proteins. C. R. Trav. Lab. Carlsberg 15:1–29, 1924.
13. Tanford, C., Kirkwood, J.G. Theory of protein titration curves. I. General equations for impenetrable spheres. J. Am. Chem. Soc. 79:5333–5339, 1957.
14. Matthew, J.B., Gurd, F.R.N., Garcia-Moreno, B., Flanagan, M.A., March, K.L., Shire, S.J. pH-dependent processes in proteins. Crit. Rev. Biochem. Mol. Biol. 18:91–197, 1985.
15. Warwicker, J., Watson, H.C. Calculation of the electric potential in the active site cleft due to α-helix dipoles. J. Mol. Biol. 157:671–679, 1982.
16. Zauhar, R.J., Morgan, R.S. A new method for computing the macromolecular electric potential. J. Mol. Biol. 186:815–820, 1985.
17. Klapper, I., Hagstrom, R., Fine, R., Sharp, K.A., Honig, B. Focusing of electric fields in the active site of Cu-Zn superoxide dismutase: Effects of ionic strength and amino-acid modification. Proteins 1:47–59, 1986.
18. Davis, M.E., Madura, J.D., Luty, B.A., McCammon, J.A. Electrostatics and diffusion of molecules in solution: Simulations with the University of Houston Brownian Dynamics program. Comput. Phys. Commun. 62:187–197, 1991.
19. Russell, S.T., Warshel, A. Calculations of electrostatic energies in proteins. The energetics of ionized groups in Bovine Pancreatic Trypsin Inhibitor. J. Mol. Biol. 185:389–404, 1985.
20. Bashford, D., Karplus, M. pKa's of ionizable groups in proteins: Atomic detail from a continuum electrostatic model. Biochemistry 29:10219–10225, 1990.
21. Bashford, D., Karplus, M. Multiple-site titration curves of proteins: An analysis of exact and approximate methods for their calculation. J. Phys. Chem. 95:9556–9561, 1991.
22. Yang, A., Honig, B. On the pH dependence of protein stability. J. Mol. Biol. 231:459–474, 1993.
23. Antosiewicz, J., McCammon, J.A., Gilson, M.K. Prediction of pH-dependent properties of proteins. J. Mol. Biol. 238: 415–436, 1994.
24. Bashford, D., Gerwert, K. Electrostatic calculations of the pK_a values of ionizable groups in bacteriorhodopsin. J. Mol. Biol. 224:473–486, 1992.
25. Beroza, P., Fredkin, D.R., Okamura, M.Y., Feher, G. Electrostatic calculations of amino acid titration and electron transfer, $Q_A^- Q_B \rightarrow Q_A Q_B^-$, in the reaction center. Biophys. J. 68:2233–2250, 1995.
26. Del Buono, G.S., Figueirido, F.E., Levy, R.M. Intrinsic pK_as of ionizable residues in proteins: An explicit solvent calculation for lysozyme. Proteins 20:85–97, 1994.
27. Lim, C., Bashford, D., Karplus, M. Absolute pK_a calculations with continuum dielectric methods. J. Phys. Chem. 95:5610–5620, 1991.

28. Simonson, T., Perahia, D., Bricogne, G. Intramolecular dielectric screening in proteins. J. Mol. Biol. 218:859–886, 1991.
29. Gibas, C.J., Subramaniam, S. Explicit solvent models in protein pK_a calculations. Biophys. J. 71:138–147, 1996.
30. Sitkoff, D., Sharp, K.A., Honig, B. Accurate calculation of hydration free energies using macroscopic solvent models. J. Phys. Chem. 98:1978–1988, 1994.
31. Bruccoleri, R.E. Grid positioning independence and the reduction of self-energy in the solution of the Poisson-Boltzmann equation. J. Comp. Chem. 14:1417–1422, 1993.
32. Oberoi, H., Allewell, N.M. Multigrid solution of the nonlinear Poisson-Boltzmann equation and calculation of titration curves. Biophys. J. 65:48–55, 1993.
33. Nina, M., Beglov, D., Roux, B. Atomic radii for continuum electrostatics calculations based on molecular dynamics free energy simulations. J. Phys. Chem. B 101:5239–5248, 1997.
34. Yang, A., Gunner, M.R., Sampogna, R., Sharp, K., Honig, B. On the calculation of pK_as in proteins. Proteins 15:252–265, 1993.
35. States, D.J., Karplus, M. A model for electrostatic effects in proteins. J. Mol. Biol. 197:122–130, 1987.
36. Demchuk, E., Wade, R.C. Improving the continuum dielectric approach to calculating pK_as of ionizable groups in proteins. J. Phys. Chem. 100:17373–17387, 1996.
37. Wendoloski, J.J., Matthew, J.B. Molecular dynamics effects on protein electrostatics. Proteins 5:313–321, 1989.
38. Northrup, S.H., Wensel, T.G., Meares, C.F., Wendoloski, J.J., Matthew, J.B. Electrostatic field around cytochrome C: Theory and energy transfer experiment. Proc. Natl. Acad. Sci. USA 87:9503–9507, 1990.
39. Langsetmo, K., Fuchs, J.A., Woodward, C., Sharp, K.A. Linkage of thioredoxin stability to titration of ionizable groups with perturbed pK_a. Biochemistry 30:7609–7614, 1991.
40. Bashford, D., Case, D.A., Dalvit, C., Tennant, L., Wright, P.E. Electrostatic calculations of side-chain pK_a values in myoglobin and comparison with NMR data for histidines. Biochemistry 32:8045–8056, 1993.
41. You, T.J., Bashford, D. Conformation and hydrogen ion titration of proteins: A continuum electrostatic model with conformational flexibility. Biophys. J. 69:1721–1733, 1995.
42. Beroza, P., Case, D.A. Including side chain flexibility in continuum electrostatic calculations of protein titration. J. Phys. Chem. 100:20156–20163, 1996.
43. Alexov, E.G., Gunner, M.R. Incorporating protein conformational flexibility into the calculation of pH-dependent protein properties. Biophys. J. 74:2075–2093, 1997.
44. Zhou, H.-X., Vijayakumar, M. Modeling of protein conformational fluctuations in pK_a predictions. J. Mol. Biol. 267: 1002–1011, 1997.
45. Nozaki, Y., Tanford, C. Examination of titration behavior. Methods Enzymol. 11:715–734, 1967.
46. Brooks, B.R., Bruccoleri, R.E., Olafson, B.D., States, D.J., Swaminathan, S., Karplus, M. CHARMM: A program for macromolecular energy, minimization and dynamics calculations. J. Comp. Chem. 4:187–217, 1983.
47. MacKerell, Jr., A.D., Bashford, D., Bellott, M., et al. All-hydrogen empirical potential for molecular modeling and dynamics studies of proteins. J. Phys. Chem. B 102: 3586–3616, 1998.
48. Beroza, P., Fredkin, D.R., Okamura, M.Y., Feher, G. Protonation of interacting residues in a protein by a Monte Carlo method: Application to lysozyme and the photosynthetic reaction center of Rhodobacter sphaeroides. Proc. Natl. Acad. Sci. USA 88:5804–5808, 1991.
49. Marquart, M., Walter, J., Deisenhofer, J., Bode, W., Huber, R. The geometry of the reactive site and of the peptide groups in trypsin, trypsinogen and its complexes with inhibitors. Acta Crystallogr. B 39:480–490, 1983.
50. Diamond, R. Real-space refinement of the structure of hen egg-white lysozyme. J. Mol. Biol. 82:371–391, 1974.
51. Wilson, K.P., Malcolm, B.A., Matthews, B.W. Structural and thermodynamic analysis of compensating mutations within the core of chicken egg white lysozyme. J. Biol. Chem. 267:10842–10849, 1992.
52. Ramanadham, M., Sieker, L.C., Jensen, L.H. Refinement of triclinic lysozyme: II. The method of stereochemically restrained least squares. Acta Crystallogr. B 46:63–69, 1990.
53. Brooks, III, C.L., Karplus, M. Solvent effects on protein motion and protein effects on solvent motion: Dynamics of the active site region of lysozyme. J. Mol. Biol. 208:159–181, 1989.
54. Brooks, III, C.L., Karplus, M. Deformable stochastic boundaries in molecular dynamics. J. Chem. Phys. 79:6312–6325, 1983.
55. Pomès, R., McCammon, J.A. Mass and step length optimization for the calculation of equilibrium properties by molecular dynamics simulation. Chem. Phys. Lett. 166:425–428, 1990.
56. Brown, L.R., De Marco, A., Wagner, G., Wüthrich, K. A study of the lysyl residues in the basic pancreatic trypsin inhibitor using ^1H nuclear magnetic resonance at 360 MHz. Eur. J. Biochem. 62:103–107, 1976.
57. Brown, L.R., De Marco, A., Richarz, R., Wagner, G., Wüthrich, K. The influence of a single salt bridge on static and dynamic features of the globular solution conformation of the basic pancreatic trypsin inhibitor. Eur. J. Biochem. 88:87–95, 1978.
58. Richarz, R., Wüthrich, K. High-field ^{13}C nuclear magnetic resonance studies at 90.5 MHz of the basic pancreatic trypsin inhibitor. Biochemistry 17:2263–2269, 1978.
59. Kuramitsu, S., Hamaguchi, K. Analysis of the acid-base titration curve of hen lysozyme. J. Biochem. 87:1215–1219, 1980.
60. Bartik, K., Redfield, C., Dobson, C.M. Measurement of the individual pK_a values of acidic residues of hen and turkey lysozymes by two-dimensional ^1H NMR. Biophys. J. 66: 1180–1184, 1994.
61. Tanokura, M. ^1H-NMR study on the tautomerism of the imidazole ring of histidine residues: I. Microscopic pK values and molar ratios of tautomers in histidine-containing peptides. Biochim. Biophys. Acta 742:576–585, 1983.